Lipogenesis and innate immunity in hepatocellular carcinoma cells reprogrammed by an isoenzyme switch of hexokinases

Laure Perrin-Cocon[1,†], Pierre-Olivier Vidalain[1,†], Clémence Jacquemin[1], Anne Aublin-Gex[1], Keedrian Olmstead[2], Baptiste Panthu[1,3], Gilles J. P. Rautureau[4], Patrice André[1], Piotr Nyczka[5], Marc-Thorsten Hütt[5], Nivea Amoedo[6], Rodrigue Rossignol[6,7], Fabian Volker Filipp[2,8], Vincent Lotteau[1,*‡] Olivier Diaz[1,*‡]

1- CIRI, Centre International de Recherche en Infectiologie, Univ Lyon, Inserm, U1111, Université Claude Bernard Lyon 1, CNRS, UMR5308, ENS de Lyon, 21 Avenue Tony Garnier, F-69007, Lyon, France.
2- Cancer Systems Biology, Institute of Computational Biology, Helmholtz Zentrum München, Ingolstädter Landstraße 1, D-85764, München, Germany.
3- Actual address: Univ Lyon, CarMeN Laboratory, Inserm, INRA, INSA Lyon, Université Claude Bernard Lyon 1, F-69921, Oullins Cedex, France.
4- Université de Lyon, CNRS, Université Claude Bernard Lyon 1, ENS de Lyon, Centre de RMN à Très Hauts Champs (CRMN), FRE 2034, F-69100 Villeurbanne, France.
5- Department of Life Sciences and Chemistry, Jacobs University, Bremen, Germany.
6- CELLOMET, Centre de Génomique Fonctionnelle de Bordeaux, 146 Rue Léo Saignat, F-33000 Bordeaux, France.
7- Univ. Bordeaux, Inserm, MRGM, U1211, F-33076, Bordeaux, France.
8- School of Life Sciences Weihenstephan, Technical University München, Maximus-von-Imhof-Forum 3, D-85354, Freising, Germany.

† These authors contributed equally to this work
‡These authors jointly supervised this work

*** Corresponding authors:**
vincent.lotteau@inserm.fr (ORCID: 0000-0003-0997-3282)
olivier.diaz@inserm.fr (ORCID: 0000-0002-3451-9914)

Classification
Major: BIOLOGICAL SCIENCES
Minor: Cell Biology

Keywords
Hepatocellular carcinoma, hexokinase, lipogenesis, innate immunity, lipoproteins.

Author Contributions
L.P-C., P-O.V., O.D., V.L. designed the experiments with critical advices from G.J.P.R., P.A., R.R. and F.V.F.; C.J., A.A-G., K.O., B.P., G.J.P.R., N.A, R.R. and F.V.F. performed experiments and analyzed the data; P.N. and M-T.H. performed metabolic network computational analysis; L.P-C., P-O.V., P.A., F.V.F, V.L. and O.D. analyzed the data, prepared figures and wrote the manuscript.

This PDF file includes:
Main Text
Figures 1 to 7

Abstract

Hexokinases catalyze the first step of glycolysis by phosphorylating glucose. In the liver, normal hepatocytes express the low-affinity hexokinase 4, also known as glucokinase (GCK), which is adapting hepatocyte function to glycaemia. Conversely, hepatocellular carcinoma (HCC) cells express the high-affinity hexokinase 2 (HK2) to sustain tumor proliferation even at low glucose concentrations. A switch from GCK to HK2 isoenzymes is occurring during the transition from primary hepatocytes to HCC. HK2 induction is a recurrent event in the carcinogenic process and relates to the highly glycolytic phenotype of HCC but the consequence of GCK loss is unknown. To explore functional consequences of the *GCK*-to-*HK2* isoenzyme switch, *HK2* was knocked-out in the HCC cell line Huh7 and replaced by *GCK,* to generate the Huh7-$GCK^{+}/HK2^{-}$ cell line. We then compared the transcriptomic, metabolomic and immunological profiles of both cell lines. The analysis of transcriptomic data from human HCC tumors shows that GCK and HK2 expression levels are inversely correlated and associated with patient survival. The replacement of HK2 by GCK rewired central carbon metabolism and restored some essential metabolic functions of normal hepatocytes such as lipogenesis, VLDL secretion and glycogen storage. It also reactivated innate immune responses and sensitivity to NK lysis. Our results suggest that the GCK-to-HK2 isoenzyme switch is playing a key role in dedifferentiation and immune escape of HCC cells.

Significance Statement

During the cancerous transformation of normal liver hepatocytes into HCC cells, the enzyme catalyzing the first rate-limiting step of glycolysis, namely GCK, is replaced by the higher affinity

isoenzyme HK2. As such, high expression level of HK2 in tumoral lesions is inversely correlated to GCK expression, and is associated to poor prognosis. We analyzed the transcriptomic, metabolomic and immune consequences of this GCK-to-HK2 isoenzyme switch by replacing HK2 by GCK in the HCC cell line Huh7. We discovered that *HK2* knockdown and *GCK* expression restores essential metabolic and immune functions of normal hepatocytes, highlighting the role of both GCK loss and HK2 induction in the natural history of HCC.

Main Text

Introduction

Hepatocellular carcinoma (HCC) is the most common liver cancer and the fourth leading cause of cancer-related death (1). HCC is closely linked to chronic liver inflammation, chronic viral hepatitis, exposure to toxins, and metabolic dysfunction such as non-alcoholic steatohepatitis (NASH). HCC is of poor prognosis, and treatments are essentially based on surgical resection, liver transplantation or aggressive chemo and/or radiotherapy. In patients with advanced HCC, broad-spectrum kinase inhibitors are approved (2) but with limited benefit (3). Effective personalized therapies are needed but their development is impeded by our poor understanding of molecular mechanisms underlying HCC onset and progression. Efforts to characterize the disease on the basis of etiology and outcomes revealed metabolic deregulation as a hallmark of HCC-subtypes progression (4). Indeed, metabolic remodeling is critically required for tumor growth as energy demand and anabolic needs drastically increase (5–7). For example, HCC cells have lost their ability to secrete VLDL, a highly specialized function acquired during hepatocyte differentiation and can only secrete LDL-like lipoproteins, indicating a defective lipogenesis and/or lipoprotein assembly (8).

Metabolic reprogramming in cancer cells involves the modulation of several enzymes by oncogenic drivers (6). Targeting these enzymes is now considered as a therapeutic strategy for several types of cancers (6). Among these enzymes, hexokinase 2 (HK2) stands out because of its elevated or induced expression in numerous cancers, including HCC (9). Hexokinases control the first rate-limiting step of glucose catabolism by phosphorylating glucose to glucose-6-phosphate (G6P), fueling glycolysis as well as glycogen, pentose phosphate and triglyceride synthesis. The human genome contains four genes encoding distinct hexokinase isoenzymes, named HK1 to HK4 (HK4 is also known as glucokinase or GCK), with distinct enzymatic kinetics and tissue distributions. A fifth putative hexokinase enzyme was recently discovered but has not been fully characterized yet (10). A switch from GCK to HK2 isoenzymes is occurring during the transition from primary to tumor hepatocytes so that HCC cell lines express HK2 but no longer GCK. HK2 expression level has been correlated with disease progression and dedifferentiation of HCC cells (11). When HK2 is artificially knocked-down in HCC cell lines, glycolysis is repressed, and tumorigenesis is inhibited while cell death increases (9). In addition, hexokinase function extends beyond metabolism towards autophagy, cell migration, and immunity, suggesting that the *GCK*-to-*HK2* isoenzyme switch has broader consequences than initially suspected (12–15). Here, we analyzed transcriptomic data of HCC biopsies and correlated hexokinase isoenzyme expression level with patient survival. This led us to generate a new human HCC cell line expressing GCK instead of HK2. A comparative analysis of GCK^+ *vs* $HK2^+$ HCC cell lines provided a unique opportunity to look into HK isoenzyme-dependent metabolic features, lipoprotein production and resistance to immune signals of liver cancer cells.

Results

Relative expression level of GCK and HK2 stratifies HCC patients

Although the isoenzyme switch from GCK to HK2 is observed during the carcinogenesis process (16), the relative expression of hexokinase isoenzymes in the tumors is unclear. We first analyzed the transcriptomes (RNAseq data) of 365 HCC biopsies from The Cancer Genome Atlas (TCGA) database (17, 18). All tumors were positive for HK1, whereas 348, 362 and 172 were positive for HK2, HK3, and GCK, respectively. Kaplan-Meyer curves show that HK1 or HK3 expression level does not correlate with the patients' survival rate (Fig. 1A). In contrast, high expression of HK2 and low expression of GCK in the tumors both correlate with a lower survival rate. In addition, HK2 expression is inversely correlated with GCK expression, suggesting a mutually exclusive setting of HK2 and GCK expression (Fig. 1B and table S1). A few patients have an exclusive HK2 profile (*i.e.* 47 patients, 12.9%) whereas the large majority shows a gradation of the GCK/HK2 expression ratio. These data indicate that expression of GCK or HK2 in HCC tumors is strongly associated with clinical outcome.

Engineering a cellular model of the hexokinase isoenzyme switch

To decipher the functional consequences of GCK or HK2 expression in a cancerous hepatocyte, we restored GCK expression by lentiviral transduction in the reference HCC cell line Huh7, and knocked-out the endogenous HK2 gene by CRISPR/Cas9. The exclusive expression of HK2 and GCK in Huh7 and Huh7-*GCK*$^{+}$/*HK2*$^{-}$ cell lines, respectively, was validated (Fig. 2A). The hexokinase activity in the presence of increasing concentration of glucose was determined in protein lysates from the two cell lines. Hexokinase activity in Huh7 lysate reached its maximum at low glucose concentration, presenting a standard Michaelis–Menten saturation curve (Fig. 2B). In contrast, the hexokinase activity in Huh7-*GCK*$^{+}$/*HK2*$^{-}$ lysates followed the expected pseudo-allosteric response to glucose (19, 20). Thus, the expected HK2 and GCK activities were observed in the Huh7 and Huh7-*GCK*$^{+}$/*HK2*$^{-}$ cells respectively. We then compared the new Huh7-*GCK*$^{+}$/*HK2*$^{-}$ and

the parental Huh7 cell lines (*i.e.* Huh7-*GCK*$^{-}$/*HK2*$^{+}$) at a transcriptomic, metabolic and immunological level.

Cellular movement and lipid metabolism distinguish Huh7 and Huh7-*GCK*$^{+}$/*HK2*$^{-}$

Transcriptomic profiles of Huh7 and Huh7-*GCK*$^{+}$/*HK2*$^{-}$ cells were determined by next generation sequencing (Table S2). Overall, 3.8% of the gene transcripts were reduced and 5.1% were induced in Huh7-*GCK*$^{+}$/*HK2*$^{-}$ compared to Huh7 (Fig. 2C; |fold-change (FC)|>2 and *p*-value<0.05). Enrichment of molecular and cellular functions in differentially expressed genes using Ingenuity Pathway Analysis (IPA) revealed that cellular movement and lipid metabolism are the most affected functions (Fig. 2D and Table S3). A closer look at these annotations pointed to differences in the migratory capacities (Fig. 2E) as well as lipid concentration and synthesis (Fig. 2F). The migratory capacities of Huh7 and Huh7-*GCK*$^{+}$/*HK2*$^{-}$ were compared using transwell-migration cell assays (Fig. 2G). Results showed a higher migratory capacity of Huh7-*GCK*$^{+}$/*HK2*$^{-}$ cells, in line with Kishore M. et al showing that GCK expression induced by pro-migratory signals controls the trafficking of Treg cells (15). To validate the differences in lipid metabolism highlighted by the transcriptomic analysis, intracellular content in neutral lipids was first determined with lipophilic dyes. As assessed by Oil-Red-O staining or BODIPY staining, an accumulation of intracellular neutral lipids is observed in Huh7-*GCK*$^{+}$/*HK2*$^{-}$ in comparison to Huh7 (Fig. 2I and J). Therefore, the hexokinase isoenzyme switch resulted in lipid droplet accumulation in Huh7-*GCK*$^{+}$/*HK2*$^{-}$ cells.

Differential lipid metabolism in Huh7 and Huh7-*GCK*$^{+}$/*HK2*$^{-}$

The intracellular lipid content of the two cell lines was further analyzed. In Huh7-*GCK*$^{+}$/*HK2*$^{-}$, an enrichment in phosphatidylcholine, cholesterol, triglycerides (TG) and free fatty acids was observed compared to Huh7 (Fig. 3A). One major function of hepatocytes is to secrete

triglyceride-rich VLDL and this function is altered in HCC cells that secrete smaller lipoproteins with the density of LDL (21, 22). The secretion of lipids and lipoproteins by both cell lines was analyzed after a 24h-culture in the absence of FCS to exclude any participation of exogenous lipids in the production of lipoproteins. Huh7-*GCK*$^{+}$/*HK2*$^{-}$ secreted more free fatty acids than Huh7 while secretion of cholesterol and TG remained unchanged (Fig. 3B). However, under the same conditions, the secretion of apolipoprotein B (ApoB) by Huh7-*GCK*$^{+}$/*HK2*$^{-}$ was reduced compared to Huh7. Since ApoB is a non-exchangeable protein with only one copy in VLDL and LDL particles, an elevated TG/ApoB ratio indicates that ApoB^{+}-lipoproteins secreted by Huh7-*GCK*$^{+}$/*HK2*$^{-}$ cells are enriched in TG compared to those secreted by Huh7 (Fig. 3C). This was confirmed by the ApoB distribution in density gradient fractions showing a secretion of LDL by Huh7 and VLDL by Huh7-*GCK*$^{+}$/*HK2*$^{-}$ (Fig. 3D). This indicates that GCK expression is essential for VLDL assembly/secretion pathway and could explain the loss of this crucial metabolic pathway in hepatoma cells expressing HK2 instead of GCK (23).

Differential activity of the tricarboxylic acid cycle (TCA) in Huh7 and Huh7-*GCK*$^{+}$/*HK2*$^{-}$

We observed that GCK expression induced lipogenesis, resulting in intracellular accumulation of lipid droplets and secretion of VLDL. A rewiring of cellular metabolism towards energy storage in Huh7-*GCK*$^{+}$/*HK2*$^{-}$ was thus suspected and confirmed by the accumulation of glycogen, creatinine and creatinine-P (Fig. 4A and B), a feature of functional hepatocytes. To determine the consequences of replacing HK2 by GCK, we quantified prominent intracellular metabolites via GC-MS. Figure 4C shows relative intracellular quantities of metabolites that are significantly different between Huh7 and Huh7-*GCK*$^{+}$/*HK2*$^{-}$. Higher levels of glucose and lactic acid were detected in Huh7-*GCK*$^{+}$/*HK2*$^{-}$. Among differentially represented metabolites, we identified several intermediates of the TCA cycle (succinic acid, fumaric acid, alpha-ketoglutaric acid), and

metabolites directly connected to it (GABA, glutamic acid, glutamine, aspartic acid). This supports a significant modulation of central carbon metabolism at both the level of glycolysis and TCA cycle. Other metabolic pathways were also modified such as nucleoside/nucleotide metabolism as assessed by changes in uracil, thymine, adenosine, adenine and 2-deoxyribose-5-phosphate levels. Higher intracellular creatinine was confirmed in cells expressing GCK. Interestingly, glycerol-3-phosphate, an intermediate of phospholipids and TG biosynthesis, was also increased in Huh7-*GCK*$^{+}$*/HK2*$^{-}$, in line with TG and phosphatidylcholine accumulation (Fig. 3A) and an activated lipogenesis pathway.

Pyruvate entering the mitochondria downstream of glycolysis can be either oxidized by pyruvate dehydrogenase (PDH), producing acetyl-CoA, or converted into oxaloacetate (OAA) by pyruvate carboxylase (PC). Acetyl-CoA and OAA are then combined in the TCA cycle to form citrate. *De novo* lipogenesis requires citrate egress from the TCA cycle to serve as a precursor of cytosolic acetyl-CoA for further synthesis of fatty acids. In Huh7-*GCK*$^{+}$*/HK2*$^{-}$ cells, we observed both an increased activity of PC (Fig. 4D) without changes in protein expression (Fig. 4E) and an increased phosphorylation of pyruvate dehydrogenase (PDH), which is indicative of a reduced activity of this enzyme (Fig. 4F). This is consistent with the increased expression of the PDH kinase PDK2 and the decreased expression of the PDH phosphatase PDP2 in Huh7-*GCK*$^{+}$*/HK2*$^{-}$ cells that regulate the PDH phosphorylation state (Fig. 4G). A rebalanced usage of pyruvate in Huh7-*GCK*$^{+}$*/HK2*$^{-}$ cells maintains a functional TCA cycle and supports lipogenesis. In Huh7-*GCK*$^{+}$*/HK2*$^{-}$ cells, we also observed an increased phosphorylation of ATP citrate lyase (ACLY), the first enzyme of the fatty acid synthesis pathway, indicating an enhanced activity of this enzyme (Fig. 4H). This reaction also regenerates OAA in the cytosolic compartment. Interestingly,

transcriptomic data show that PCK1 which converts OAA to PEP, a precursor of glycerol-3-phosphate for TG synthesis, is expressed in Huh7-*GCK*$^{+}$/*HK2*$^{-}$cells but not in Huh7.

A shift from pyruvate oxidation to carboxylation is observed in cancer cells where succinate dehydrogenase (SDH) is inactivated by mutation and OAA can only be generated through PC activity (24). SDH inhibition leads to succinate accumulation, especially in activated immune cells (25). Interestingly, higher levels of succinate and a reduced activity of SDH were measured in Huh7-*GCK*$^{+}$/*HK2*$^{-}$ cells compared to Huh7 (Fig. 4I & 4J). Even though SDH is also part of the complex II of the mitochondrial respiratory chain, we observed that oxygen consumption is increased in Huh7-*GCK*$^{+}$/*HK2*$^{-}$ (Fig. 4K), suggesting that other pathways maintain a high activity of the respiratory chain by fueling complex III. Thereby, the HK isoenzyme switch rewired the TCA cycle promoting carboxylation of pyruvate into OAA in the presence of a reduced SDH activity.

Gene-centric metabolic analysis of transcriptomic data revealed extended modifications of metabolic connections

The metabolic consequences of the HK isoenzyme switch can also be determined from the transcriptome profiles by mapping the differentially expressed genes onto reference metabolic networks and extracting highly-connected subgraphs (Methods and Fig. S1-4). Recon2 and HepatoNet1, two well-established bipartite metabolic networks connecting gene products and metabolites, were used as framework (26). Highest-degree metabolites were first removed as currency metabolites, each network was simplified by bipartite network projection to obtain gene-centric networks (*i.e.* without metabolites) and transcriptomic data were used to filter these gene-centric networks. The optimal expression fold-change was set according to the best connectivity score obtained for the resulting subgraphs (Methods and Fig. S1-4). Clusters of

genes that are both differentially expressed and connected by common metabolites emerge from this analysis, highlighting metabolic modules that distinguish Huh7 from Huh7-*GCK*$^{+}$/*HK2*$^{-}$. Interestingly, we found that across a wide range of analysis parameters, including varying rates of currency metabolites and gene expression fold-change, the differentially expressed genes are substantially better connected in the HepatoNet1 metabolic model of liver cells than in the generic human metabolic model Recon2 (Fig. S4). This highlights the specificity of the transcriptomic changes with respect to hepatocyte metabolism. To obtain the spanned network presented in Fig. 5, we applied to the liver model HepatoNet1 an optimal fold-change threshold of 2 for transcriptomic data and removed 5 percent of highest-degree currency metabolites (thus retaining 95 percent of metabolites). The effective network spanned by the differentially expressed genes shows connected components within and between lipid metabolic clusters, reinforcing our above data, but also hexoses, nucleotides and amino acids pathways. It also shows modifications in gene expression amongst the connected clusters pyruvate/malate, mevalonate, one-carbon pathways and urea cycle. This analysis highlights the global impact of the HK isoenzyme switch that spreads way beyond glycolysis and across distant connected metabolic modules.

Restored immune sensitivity in Huh7-*GCK*$^{+}$/*HK2*$^{-}$

Lipid accumulation in hepatocytes is incriminated in hepatic inflammation (27) and TCA cycle rewiring is associated with innate immunity activation (28). These two events were observed when replacing HK2 by GCK in Huh7 cells, questioning the immune status of these cells and their sensitivity to antitumor immunity. By analyzing transcriptomic data with the GO term “Type I-IFN signaling pathway”, we observed that amongst the 91 genes of this GO term, 17 were significantly up-regulated in Huh7-*GCK*$^{+}$/*HK2*$^{-}$ compared to Huh7 (Fig. 6A). This includes IRF1, 7

and 9, three crucial transcription factors, IFN-stimulated genes (ISGs) such as Mx1, OAS1, OAS3 and signaling intermediates such as IKBKE (IKKε gene) (Fig. 6B). Among the members of the RIG-like receptor (RLR) family involved in immune sensing and antitumor defense (29), the expression of MDA5 (IFIH1 gene) was slightly higher in Huh7-*GCK*$^{+}$/*HK2*$^{-}$ whereas that of RIG-I was unchanged. These results suggested that Huh7-*GCK*$^{+}$/*HK2*$^{-}$ cells may be better equipped than Huh7 cells to respond to immune signals. We thus compared the immune response of the two cell lines when stimulated by RIG-I or MDA5 ligands, by transfecting triphosphate-hairpin RNA (3p-hpRNA) or poly(I:C) respectively. ISRE-dependent transcription was efficiently induced by RLR ligands in Huh7-*GCK*$^{+}$/*HK2*$^{-}$ cells whereas Huh7 response was very limited even at high doses of ligands (Fig. 6C).

To investigate whether this differential sensitivity to RLR ligands is linked to GCK expression or HK2 knockout, we used Huh7-derived cells transduced for GCK expression so that they express both HK2 and GCK (Huh7-*GCK*$^{+}$/*HK2*$^{+}$). In these cells, the response to RIG-I ligation did not differ from that of Huh7 cells suggesting that GCK expression alone is not sufficient to restore immune sensitivity (Fig. 6D). When HK2 expression was repressed in these cells with a shRNA (Huh7-*GCK*$^{+}$/*HK2*$^{-}$Sh) (see Fig. S5 showing 95% extinction of HK2 protein), ISRE response to RIG-I signaling was restored to a level similar to that observed in Huh7-*GCK*$^{+}$/*HK2*$^{-}$ cells (Fig. 6D). This is pointing towards HK2 as a negative regulator of RLR signaling in HCC cells and strongly suggests that the *GCK*-to-*HK2* isoenzyme switch during malignant transformation of hepatocytes is accompanied by a reduced sensitivity to immune signals that could favor escape to immune surveillance. The higher sensitivity to RLR ligands of Huh7-*GCK*$^{+}$/*HK2*$^{-}$ cells also resulted in increased secretion of inflammatory (IL-6 and IL-8) and antiviral cytokines (IFN-λ_1, IFN-$\lambda_{2/3}$, IFN-β and IP-10) (Fig. 6E), indicating that both NF-κB and IRF3 dependent signaling pathways were

induced. IL-1β, TNFα, IL-12p70, GM-CSF, IL-10 and IFNγ were not detected in the supernatants of none of the cell lines, whether they were stimulated or not.

As NK cell-mediated lysis of tumor cells is crucial for the anti-cancer immune defense, we compared the susceptibility of the two cell lines to NK cells cytotoxicity. Figure 6F shows that Huh7 cells are resistant to NK cell-mediated lysis in contrast to Huh7-*GCK*$^{+}$/*HK2*$^{-}$. Thus, replacing HK2 by GCK restored Huh7 sensitivity to NK cell-mediated lysis. Similar results were obtained when NK cells were pre-activated with IL-2 (Fig. S6). Altogether, these results demonstrate that HCC cells expressing HK2 instead of GCK exhibit an impaired response to immune signals and also a strong resistance to NK cells. Significantly, these two observations are in line with clinical data showing that elevated GCK expression is associated with prolonged survival, while elevated HK2 expression coinciding with GCK reduction correlates with shorter overall survival (Fig. 1).

Discussion

Metabolic network rewiring is a hallmark of cancer although for most tumors, mechanisms at the origin of this metabolic reprogramming have not been elucidated. While GCK, but not HK2, is expressed in normal hepatocytes, the expression of HK2 occurs during cirrhosis and increases as the disease progresses to carcinoma (16). Analyzing TCGA data from human HCC tumors, we observed that HK2 and GCK expression is inversely correlated and that high HK2/GCK ratio is of poor prognosis. On the contrary, HK1 and HK3 expression levels were not correlated to patient survival. As HK2 and GCK expression tend to be mutually exclusive, both HK2 induction and GCK downregulation might have consequences on the metabolic reprogramming during malignant transformation of hepatocytes. To compare the functional consequences of the HK isoenzyme switch in HCC, we therefore expressed GCK in the reference HCC cell line Huh7 and knocked-down HK2 expression. Our comparative transcriptomic, metabolic and functional studies

demonstrate that the replacement of HK2 by GCK not only restored some essential metabolic functions of normal hepatocytes such as lipogenesis, VLDL secretion and glycogen storage but also reactivated innate immune responses and sensitivity to NK lysis.

HCC cell lines predominantly secrete LDL-like particles, unlike normal hepatocytes that secrete VLDL. Lipid loading of Huh7 cells with oleic acid can boost the secretion of $ApoB^+$ particles but does not induce a shift from LDL to VLDL density, indicating that intracellular fatty acid accumulation of exogenous origin cannot rescue VLDL production (23). Here we show that replacing HK2 by GCK in Huh7 cells restored *de novo* fatty acid synthesis, allowing VLDL assembly/secretion in the absence of exogenous lipids. To our knowledge Huh7-$GCK^+/HK2^-$ is the first human cell line with a functional VLDL secretion pathway that should strongly benefit the field of cardiovascular diseases and hepatic steatosis.

De novo fatty acid synthesis from carbohydrates requires an adequate supply in metabolic substrates, especially citrate produced by the TCA cycle. The glycolytic entry point into the TCA cycle is controlled by PDH and PC that convert pyruvate into acetyl-CoA or OAA, respectively. Our data revealed that PC activity is increased in contrast to PDH that is inhibited, suggesting that pyruvate metabolism is rebalanced in favor of OAA in Huh7-$GCK^+/HK2^-$ cells, as described in healthy liver. Such a mechanism of anaplerosis is known to replenish TCA cycle intermediates and compensate citrate export out of the mitochondria for lipogenesis fueling. Increased PC activity is observed in both normal and pathological situations, mainly as a result of an increased transcription of the PC gene. In our model, mRNA and protein levels were not affected, indicating that PC activity can be regulated by alternative mechanisms depending on HK isoenzyme expression.

A rebalanced pyruvate usage in favor of OAA is also described for instance for SDH-deficient neuroendocrine tumor cells, where succinate accumulates and PC activity is increased to maintain OAA production, replenish the oxidative TCA cycle and support aspartate synthesis (24). Interestingly, in comparison to Huh7 cells, succinate and aspartate levels are elevated in Huh7-*GCK*$^{+}$/*HK2*$^{-}$ where SDH activity is reduced, suggesting a direct link between PC and SDH activity in hepatocytes.

Several mechanisms inhibiting SDH have been described (30). Modification of the expression of SDH subunits is unlikely as no variation was observed at the transcriptomic level. Itaconate is a weak inhibitor of SDH produced by IRG1 from aconitate but this metabolite was not detected and IRG1 mRNA was absent from the transcriptome of both cell lines. Whether fumarate or other metabolites are responsible for the reduced SDH activity in GCK-expressing cells remains to be investigated.

SDH-deficient cells and LPS-Stimulated macrophages have been shown to elicit a hypoxic-like phenotype through accumulation of large amounts of succinate and stabilization of HIF-1α (31, 32). Despite an elevated succinate steady-state level in Huh7-*GCK*$^{+}$/*HK2*$^{-}$ compared to Huh7 cells, we observed no difference in HIF-1α stabilization neither at basal level nor upon induction (Fig. S7). This suggested that the reduction of SDH activity in Huh7-*GCK*$^{+}$/*HK2*$^{-}$ cells was not strong enough to induce a pseudo-hypoxic phenotype.

Our gene-centric metabolic analysis of transcriptomic data revealed a wide spreading of metabolic modifications resulting from HK isoenzyme switch. Illustrating these modifications, Figure 7 is an attempt to integrate the observed changes in central carbon metabolism and closely connected metabolic pathways. In particular, decreased level of alanine and increased aspartate concentration in Huh7-*GCK*$^{+}$/*HK2*$^{-}$ cells could be an indirect effect of PC activation that

uses pyruvate for the synthesis of OAA. As a consequence, hepatic transaminases may balance intracellular pools of OAA, aspartate, alanine and pyruvate. Glutamate and GABA levels were also modified, thus supporting anaplerosis of the TCA cycle through glutamine consumption and the GABA shunt pathway, respectively. We also observed lower levels of oxalate, an end-product of glyoxylate degradation. Increased levels of the enzyme AGXT (serine-pyruvate aminotransferase) could account for this phenotype as it converts alanine and glyoxylate into pyruvate and glycine which is also increased. Interestingly, high level of AGXT is a good prognostic marker for HCC (33). We also observed that isoleucine and valine levels increased while the expression of BCAT1 (Branched Chain Amino Acid Transaminase 1) decreased. This suggests a reduced catabolism of branched chain amino acids in Huh7-*GCK*$^{+}$/*HK2*$^{-}$ cells. Again, low levels of BCAT1 is a good prognostic marker for HCC and oral supplementation with branched chain amino acids has been shown to reduce the risk of liver cancer in cirrhotic patients (34, 35). If some metabolic modifications seem to advocate for the restoration of a normal hepatocyte phenotype following the replacement of HK2 by GCK, it cannot be a general statement. Indeed, the urea cycle was also impacted in Huh7-*GCK*$^{+}$/*HK2*$^{-}$ cells with lower levels of CPS1 and OTC, which are also observed in aggressive HCC tumors (36). Altogether, our results demonstrate the broad impact of replacing HK2 by GCK in HCC cells, and the key role played by the HK isoenzyme switch in HCC tumor metabolism.

We discovered that HK isoenzyme expression not only controls hepatic metabolic functions but also interferes with intrinsic innate immunity of hepatocytes and antitumoral immune surveillance. Several reports have recently established functional links between glucose metabolism and signaling pathways downstream of innate immunity sensors of the RLR family, RIG-I and MDA5 (37–39), which are usually associated with antiviral responses. However, RIG-I

expression is downregulated in hepatic cancer tissues and low RIG-I expression is correlated with poor survival of patients, whereas RIG-I expression in HCC cell lines enhanced IFN response and cancer cell apoptosis (29). This suggests an unexpected role of this receptor family in the antitumoral response. Here we show that Huh7 cells expressing GCK instead of HK2 exhibit a higher sensitivity to RIG-I and MDA5 ligands, and produce higher levels of type I/III IFNs and inflammatory cytokines. Interestingly, it has been shown recently that glucose metabolism, which drives not only glycolysis but also the hexosamine biosynthetic pathway, promotes MAVS signaling through the generation of UDP-GlcNAc (37). This metabolite is crucial to the O-GlcNAcylation and activation of MAVS, the mitochondrial signaling adaptor downstream RIG-I and MDA5 (37). Thus, an intriguing hypothesis is that GCK expression could facilitate MAVS signaling by upregulating the hexosamine biosynthetic pathway. HK2 binding at the surface of mitochondria may also compete with pyruvate carboxylase, metabolites or mitochondria factors known to control MAVS signaling (37–39). Further investigations are now required to decipher the molecular mechanisms involved.

Beyond the inhibition of RLR signaling, other mechanisms might contribute to tumor escape from immune surveillance in HCC patients. In advanced-stage HCC patients, NK cells often exhibit reduced infiltration and impaired functional activities (40). We thus compared the sensitivity of Huh7-*GCK*$^{+}$/*HK2*$^{-}$ cells to Huh7, and found that sensitivity to NK cell lysis is restored when HK2 is replaced by GCK. When analyzing cell surface expression of HLA class I molecules and MICA/B, no significant changes were observed between cell lines (Fig. S6). In contrast, an increased ICAM-1 transcription and surface expression (FC=2.6; Fig. S6) were observed in Huh7-*GCK*$^{+}$/*HK2*$^{-}$. Since ICAM-1 binding to active LFA-1 at the surface of NK cells is essential for granule polarization and efficient killing of the target cells (41), its enhanced exposition at the surface of

Huh7-*GCK*$^{+}$/*HK2*$^{-}$ may contribute to their higher sensitivity to NK cell-mediated killing. These results suggest that HK2 expression at the expense of GCK in HCC tumors decreases immune responsiveness and sensitivity to NK cytotoxicity, thus favoring immune escape. Overall our data indicate that HK2 and GCK isoenzymes play a crucial role in establishing the metabolic and immune status of hepatocytes during their malignant transformation.

Materials and Methods

Materials. Unless otherwise specified, chemicals were from Merck Sigma-Aldrich. The RIG-I specific ligand 3p-hpRNA and the MDA5/TLR3 ligand poly(I:C) HMW (High Molecular Weight) were from Invivogen.

Cell cultures. Huh7 cells and derivatives were grown as previously described (42) in DMEM, 10% fetal calf serum (FCS), penicillin/streptomycin, 1mM pyruvate, 2mM L-glutamine. Culture medium and additives were from Gibco except FCS (Dominique Dutcher).

Cell lines. 15.10^{4} Huh7 cells were transduced for GCK expression at different multiplicities of infection (lentiviral transduction using the pLEX-GCK construct). The Huh7-*GCK*$^{+}$/*HK2*$^{+}$ cells were then cultured for 7 days with puromycin (1µg/mL) before amplification. HK2 knock-out was achieved using the CRISPR/Cas9 system as previously described (43) to obtain Huh7-*GCK*$^{+}$/*HK2*$^{-}$ cells. A single guide RNA (sgRNA) pair was designed for double nicking using the CRISPR Design Tool (http://tools.genome-engineering.org). The guide sequence oligos (sgRNA$_1$(*HK2*): 5'-CACCGTGACCACATTGCCGAATGCC-3' and sgRNA$_2$(*HK2*): 5'-CACCGTTACCTCGTCTAGTTTAGTC-3') were cloned into a plasmid containing sequences for Cas9 expression and the sgRNA scaffold (pSpCas9(BB)-2A-GFP, Addgene plasmid #48138). 48h post-transfection, cells were sorted by FACS based on the transient expression of GFP and cloned by limiting dilution. Effective deletion of HK2 was assessed by qPCR.

For *HK2* knock-down, Huh7-*GCK*$^{+}$/*HK2*$^{+}$ cells were transduced with lentiviral vectors expressing HK2-targeting shRNAs, and antibiotic selection was applied (hygromycin; 100µg/ml). The *HK2*-targeting sequence 5'-CCGGCCAGAAGACATTAGAGCATCTCTCGAGAGATGCTCTAATGTCTTCTGGTTTTTT-3' was cloned in the pLKO.1 hygro vector (a gift from Bob Weinberg; Addgene plasmid #24150). HK2 expression in Huh7-*GCK*$^{+}$/*HK2*$^{+}$ and Huh7-*GCK*$^{+}$/*HK2*$^{-}$*Sh* was analyzed on cell lysates by western blotting (Fig. S5).

Enzymatic activity assays. Cells were trypsinized, washed twice, and cell pellets were stored at -80°C. Protein extractions and assays were performed as previously described for hexokinase (44–46) and pyruvate carboxylase (47). Specific enzymatic assays are described in Supplementary Methods.

Metabolomic profiling. Cells were seeded at 13.10^5 cells in $75cm^2$ dishes. After 24h, culture medium was replaced and cells were further incubated during 24h. Cells were harvested, washed twice with ice-cold PBS, and cell pellets were stored at -80°C. Extraction, separation and analysis of the metabolites by GC-MS are described in Supplementary Methods.

Transcriptome profiling of Huh7 and Huh7-*GCK*$^{+}$/*HK2*$^{-}$ cell lines. Transcriptome profiling was performed by next generation sequencing (Profilexpert, Lyon). Fragments per kilobases of exon per million mapped (FPKM) reads were analyzed for differential gene expression between Huh7 and Huh7-*GCK*$^{+}$/*HK2*$^{-}$ cell lines using Student's t-test with Benjamini-Hochberg correction. See Supporting Information and Gene Expression Omnibus database with the accession number GSE144214 for entire raw data.

Pathway analysis. The list of transcripts differentially expressed in Huh7 and Huh7-*GCK*$^{+}$/*HK2*$^{-}$ cell lines was analyzed by gene set enrichment analysis (IPA, Build version: 486617M, Qiagen)

weighted by their corresponding fold-change and *p*-value. The fold-change cut-off of median expression for each transcript FPKM was set at 2 with a *p*-value<0.05. The list of genes associated with "Type I-IFN signaling pathway" was defined in the AmiGO 2 database. Expression data of these genes were retrieved from the transcriptomes of Huh7-*GCK*$^{+}$/*HK2*$^{-}$ and Huh7, and correspond for each gene to the sum of FPKMs values across all splice variants.

Cell migration assay. 2.10^4 cells were plated in the upper chamber of transwells with DMEM without FCS to allow migration for 24h at 37°C. DMEM with 10% FCS was distributed in each well, below the chamber. Chambers were gently picked up before a brief PBS rinse and 0.05% crystal violet coloration. Cells at the lower position of the chamber were photographed and counted.

Respiration Assay. Respiration was measured using a XF-96 Extracellular Flux Analyzer (Seahorse Bioscience). The assay was performed according to the Agilent Seahorse XF Cell Mito Stress Test as detailed in Supplementary Methods. The number of cells was determined at the end of the run using the SRB assay as previously described (48).

Intracellular lipid staining. For microscopic observations, cells were fixed 48h post-seeding, and intracellular lipids stained with Oil-Red-O as described in Supplementary Methods. For the quantification of intracellular lipid droplets by FACS, cells were stained with the BODIPY® 493/503 dye (Tocris Bio-Techne).

Protein, ApoB, and Lipid Quantification. Protein concentration was determined using the DC Protein Assay (Bio-Rad). ApoB concentration in medium and gradients fractions was determined by ELISA as previously described (49). Total concentrations of cholesterol, phospholipids, and triglycerides (TG) were determined using specific assays from Millipore Sigma-Aldrich (ref.

MAK043, MAK122 and MAK266 respectively). Free Fatty Acids were quantified using a specific assay kit from Abcam (ref. ab65341).

Iodixanol density gradients. Iodixanol gradients were prepared as previously described (50). One ml of culture supernatant was applied to the top of 6 to 56% iodixanol gradients and centrifuged for 10h at 41,000rpm and 4°C in a SW41 rotor. The gradient was harvested by tube puncture from the bottom and collected into 22 fractions (0.5ml each). The density of each fraction was determined by weighing.

Metabolic network coherence computational analysis. In order to measure the consistency of differentially expressed genes with a metabolic network, we employed the metabolic network coherence measure introduced by Sonnenschein *et al.* (51) (see Supplementary Methods for details). This approach was previously applied to various disease-related transcriptome profiles (52, 53) and for extracting information on the genetic control of metabolic organization (54).

Western-Blot Analysis. Protein expression was determined by standard western-blot analysis (See Supplementary Methods for details).

RLR stimulation

Cells were seeded in 96-well or 24-well plates. After 24h, cells were co-transfected with indicated doses of the RIG-I ligand 3p-hpRNA or the MDA5/TLR3 ligand poly(I:C) HMW together with the pISRE-luc (1.25µg/ml) and pRL-SV40 (0.125µg/ml) reporter plasmids using the JetPEI-Hepatocyte reagent (Polyplus Transfection). Manufacturer's instructions were followed. After 48h, supernatants were collected for cytokine quantification. Firefly and Renilla luciferase expressions within cells were determined using the Dual-Glo luciferase Assay system (Promega) and an Infinite M200 microplate reader (TECAN).

Cytokine assays

Clarified culture supernatants were collected and stored at -20°C. IL-8 was quantified using the Cytometric Bead Array for human IL-8 (BD Biosciences). Other cytokines were assayed using the LEGENDPlex multiplex assay (Human Anti-Virus Response Panel, BioLegend). Fluorescence was analyzed using a FACS Canto II (BD Biosciences).

NK cell cytotoxicity test

NK cells were isolated as described in Supplementary Methods from human buffy coats of healthy donors obtained from the Etablissement Français du Sang. Informed consent was obtained from donors and experimental procedures were approved by the local institutional review committee. Huh7 or Huh7-*GCK*$^{+}$/*HK2*$^{-}$ were seeded at 1.10^5 cells per well in a 24-well plate in RPMI-1640 (Gibco) with 10% FCS and 40µg/ml gentamycin. After 24h, 3.10^5 or 3.10^6 NK cells were added to the culture wells. The cytotoxicity assay was performed for 4h at 37°C, under 5% CO_2. Target hepatoma cells were harvested after trypsination, labelled with propidium iodide (PI) and analyzed by FACS. Cell death was monitored after morphological gating on hepatocytes.

Statistics and reproducibility

All the statistical analyses were performed with GraphPad Prism or Analyse-it softwares. Details of statistical analyses can be found in figure legends.

Acknowledgments

We acknowledge the contribution of the AniRA-Cytometry and PLATIM-microscopy Core Facilities of SFR Biosciences (UMS3444/US8) and of ProfileXpert, Genomics and Microgenomics platform, University Lyon 1, SFR santé LYON-EST, UCBL-Inserm US 7-CNRS UMS 3453. This work was supported by the Fondation pour la Recherche Médicale (FRM), grant number DEQ20160334893 to VL. F.V.F. is grateful for the support by grants CA154887, GM115293, CRN-

17-427258, NSF GRFP, and the Science Alliance on Precision Medicine and Cancer Prevention by the German Federal Foreign Office, implemented by the Goethe-Institute, Washington, DC, USA, and supported by the Federation of German Industries (BDI), Berlin, Germany.

References

1. A. Villanueva, Hepatocellular Carcinoma. *N. Engl. J. Med.* **380**, 1450–1462 (2019).

2. M. Kudo, *et al.*, Lenvatinib versus sorafenib in first-line treatment of patients with unresectable hepatocellular carcinoma: a randomised phase 3 non-inferiority trial. *The Lancet* **391**, 1163–1173 (2018).

3. J. M. Llovet, R. Montal, D. Sia, R. S. Finn, Molecular therapies and precision medicine for hepatocellular carcinoma. *Nat Rev Clin Oncol* **15**, 599–616 (2018).

4. S. De Matteis, *et al.*, Aberrant Metabolism in Hepatocellular Carcinoma Provides Diagnostic and Therapeutic Opportunities. *Oxidative Medicine and Cellular Longevity* **2018**, 1–13 (2018).

5. F. V. Filipp, *et al.*, Glutamine-fueled mitochondrial metabolism is decoupled from glycolysis in melanoma. *Pigment Cell & Melanoma Research* **25**, 732–739 (2012).

6. N. Hay, Reprogramming glucose metabolism in cancer: can it be exploited for cancer therapy? *Nat Rev Cancer* **16**, 635–649 (2016).

7. M. G. Vander Heiden, L. C. Cantley, C. B. Thompson, Understanding the Warburg effect: the metabolic requirements of cell proliferation. *Science* **324**, 1029–1033 (2009).

8. J. Jiang, P. Nilsson-Ehle, N. Xu, Influence of liver cancer on lipid and lipoprotein metabolism. *Lipids Health Dis* **5**, 4 (2006).

9. D. DeWaal, *et al.*, Hexokinase-2 depletion inhibits glycolysis and induces oxidative phosphorylation in hepatocellular carcinoma and sensitizes to metformin. *Nature Communications* **9**, 446 (2018).

10. C. Guo, *et al.*, Coordinated regulatory variation associated with gestational hyperglycaemia regulates expression of the novel hexokinase HKDC1. *Nat Commun* **6**, 6069 (2015).

11. G. Guzman, *et al.*, Evidence for Heightened Hexokinase II Immunoexpression in Hepatocyte Dysplasia and Hepatocellular Carcinoma. *Dig Dis Sci* **60**, 420–426 (2015).

12. A. J. Wolf, *et al.*, Hexokinase Is an Innate Immune Receptor for the Detection of Bacterial Peptidoglycan. *Cell* **166**, 624–636 (2016).

13. V. P. Tan, S. Miyamoto, HK2/hexokinase-II integrates glycolysis and autophagy to confer cellular protection. *Autophagy* **11**, 963–964 (2015).

14. D. J. Roberts, V. P. Tan-Sah, E. Y. Ding, J. M. Smith, S. Miyamoto, Hexokinase-II Positively Regulates Glucose Starvation-Induced Autophagy through TORC1 Inhibition. *Mol. Cell* **53**, 521–533 (2014).

15. M. Kishore, *et al.*, Regulatory T Cell Migration Is Dependent on Glucokinase-Mediated Glycolysis. *Immunity* **47**, 875-889.e10 (2017).

16. N. C. W. Lee, M. A. Carella, S. Papa, C. Bubici, High Expression of Glycolytic Genes in Cirrhosis Correlates With the Risk of Developing Liver Cancer. *Front Cell Dev Biol* **6**, 138 (2018).

17. M. Uhlén, *et al.*, Tissue-based map of the human proteome. *Science* **347** (2015).

18. M. Uhlen, *et al.*, A pathology atlas of the human cancer transcriptome. *Science* **357** (2017).

19. C. M. Porter, B. G. Miller, Cooperativity in monomeric enzymes with single ligand-binding sites. *Bioorganic Chemistry* **43**, 44–50 (2012).

20. M. Larion, R. K. Salinas, L. Bruschweiler-Li, B. G. Miller, R. Brüschweiler, Order–Disorder Transitions Govern Kinetic Cooperativity and Allostery of Monomeric Human Glucokinase. *PLoS Biology* **10**, e1001452 (2012).

21. G. van den Berghe, The role of the liver in metabolic homeostasis: Implications for inborn errors of metabolism. *Journal of Inherited Metabolic Disease* **14**, 407–420 (1991).

22. J. M. Berg, J. L. Tymoczko, L. Stryer, Each Organ Has a Unique Metabolic Profile. *Biochemistry. 5th edition* (2002) (January 13, 2020).

23. S. J. R. Meex, U. Andreo, J. D. Sparks, E. A. Fisher, Huh-7 or HepG2 cells: which is the better model for studying human apolipoprotein-B100 assembly and secretion? *J. Lipid Res.* **52**, 152–158 (2011).

24. C. Lussey-Lepoutre, *et al.*, Loss of succinate dehydrogenase activity results in dependency on pyruvate carboxylation for cellular anabolism. *Nat Commun* **6**, 8784 (2015).

25. V. Lampropoulou, *et al.*, Itaconate Links Inhibition of Succinate Dehydrogenase with Macrophage Metabolic Remodeling and Regulation of Inflammation. *Cell Metab.* **24**, 158–166 (2016).

26. C. Gille, *et al.*, HepatoNet1: a comprehensive metabolic reconstruction of the human hepatocyte for the analysis of liver physiology. *Mol Syst Biol* **6**, 411 (2010).

27. A. Mansouri, C.-H. Gattolliat, T. Asselah, Mitochondrial Dysfunction and Signaling in Chronic Liver Diseases. *Gastroenterology* **155**, 629–647 (2018).

28. E. L. Mills, B. Kelly, L. A. J. O'Neill, Mitochondria are the powerhouses of immunity. *Nature Immunology* **18**, 488 (2017).

29. J. Hou, *et al.*, Hepatic RIG-I predicts survival and interferon-α therapeutic response in hepatocellular carcinoma. *Cancer Cell* **25**, 49–63 (2014).

30. J. Van den Bossche, L. A. O'Neill, D. Menon, Macrophage Immunometabolism: Where Are We (Going)? *Trends in Immunology* **38**, 395–406 (2017).

31. G. M. Tannahill, *et al.*, Succinate is an inflammatory signal that induces IL-1β through HIF-1α. *Nature* **496**, 238–242 (2013).

32. K. Kluckova, D. A. Tennant, Metabolic implications of hypoxia and pseudohypoxia in pheochromocytoma and paraganglioma. *Cell Tissue Res.* **372**, 367–378 (2018).

33. Y. Sun, *et al.*, Loss of alanine-glyoxylate and serine-pyruvate aminotransferase expression accelerated the progression of hepatocellular carcinoma and predicted poor prognosis. *J Transl Med* **17**, 390 (2019).

34. Y. Muto, *et al.*, Overweight and obesity increase the risk for liver cancer in patients with liver cirrhosis and long-term oral supplementation with branched-chain amino acid granules inhibits liver carcinogenesis in heavier patients with liver cirrhosis. *Hepatol. Res.* **35**, 204–214 (2006).

35. T. Kawaguchi, *et al.*, Branched-chain amino acids prevent hepatocarcinogenesis and prolong survival of patients with cirrhosis. *Clin. Gastroenterol. Hepatol.* **12**, 1012-1018.e1 (2014).

36. A. Ally, *et al.*, Comprehensive and Integrative Genomic Characterization of Hepatocellular Carcinoma. *Cell* **169**, 1327-1341.e23 (2017).

37. T. Li, *et al.*, O-GlcNAc Transferase Links Glucose Metabolism to MAVS-Mediated Antiviral Innate Immunity. *Cell Host Microbe* **24**, 791-803.e6 (2018).

38. W. Zhang, *et al.*, Lactate Is a Natural Suppressor of RLR Signaling by Targeting MAVS. *Cell* **178**, 176-189.e15 (2019).

39. Z. Cao, *et al.*, Pyruvate Carboxylase Activates the RIG-I-like Receptor-Mediated Antiviral Immune Response by Targeting the MAVS signalosome. *Sci Rep* **6**, 22002 (2016).

40. L. Cai, *et al.*, Functional impairment in circulating and intrahepatic NK cells and relative mechanism in hepatocellular carcinoma patients. *Clin. Immunol.* **129**, 428–437 (2008).

41. Y. T. Bryceson, M. E. March, D. F. Barber, H.-G. Ljunggren, E. O. Long, Cytolytic granule polarization and degranulation controlled by different receptors in resting NK cells. *J Exp Med* **202**, 1001–1012 (2005).

42. C. Scholtes, *et al.*, Enhancement of genotype 1 hepatitis C virus replication by bile acids through FXR. *J. Hepatol.* **48**, 192–199 (2008).

43. F. A. Ran, *et al.*, Genome engineering using the CRISPR-Cas9 system. *Nature Protocols* **8**, 2281–2308 (2013).

44. Y. Kuang, S. J. Schomisch, V. Chandramouli, Z. Lee, Hexokinase and glucose-6-phosphatase activity in woodchuck model of hepatitis virus-induced hepatocellular carcinoma. *Comp. Biochem. Physiol. C Toxicol. Pharmacol.* **143**, 225–231 (2006).

45. C. Ramière, *et al.*, Activity of hexokinase is increased by its interaction with hepatitis C virus protein NS5A. *J. Virol.* **88**, 3246–3254 (2014).

46. L. Perrin-Cocon, *et al.*, Toll-like Receptor 4-Induced Glycolytic Burst in Human Monocyte-Derived Dendritic Cells Results from p38-Dependent Stabilization of HIF-1α and Increased Hexokinase II Expression. *J. Immunol.* **201**, 1510–1521 (2018).

47. J. Payne, J. G. Morris, Pyruvate carboxylase in Rhodopseudomonas spheroides. *J. Gen. Microbiol.* **59**, 97–101 (1969).

48. P. Skehan, *et al.*, New colorimetric cytotoxicity assay for anticancer-drug screening. *J. Natl. Cancer Inst.* **82**, 1107–1112 (1990).

49. C. Scholtes, *et al.*, High plasma level of nucleocapsid-free envelope glycoprotein-positive lipoproteins in hepatitis C patients. *Hepatology* **56**, 39–48 (2012).

50. V. Icard, *et al.*, Secretion of hepatitis C virus envelope glycoproteins depends on assembly of apolipoprotein B positive lipoproteins. *PLoS ONE* **4**, e4233 (2009).

51. N. Sonnenschein, M. Geertz, G. Muskhelishvili, M.-T. Hütt, Analog regulation of metabolic demand. *BMC Syst Biol* **5**, 40 (2011).

52. N. Sonnenschein, *et al.*, A network perspective on metabolic inconsistency. *BMC Syst Biol* **6**, 41 (2012).

53. C. Knecht, C. Fretter, P. Rosenstiel, M. Krawczak, M.-T. Hütt, Distinct metabolic network states manifest in the gene expression profiles of pediatric inflammatory bowel disease patients and controls. *Sci Rep* **6**, 32584 (2016).

54. K. Schlicht, *et al.*, The metabolic network coherence of human transcriptomes is associated with genetic variation at the cadherin 18 locus. *Hum. Genet.* **138**, 375–388 (2019).

55. J. Gao, *et al.*, Integrative Analysis of Complex Cancer Genomics and Clinical Profiles Using the cBioPortal. *Sci Signal* **6**, pl1 (2013).

56. E. Cerami, *et al.*, The cBio Cancer Genomics Portal: An Open Platform for Exploring Multidimensional Cancer Genomics Data. *Cancer Discov* **2**, 401–404 (2012).

Figures

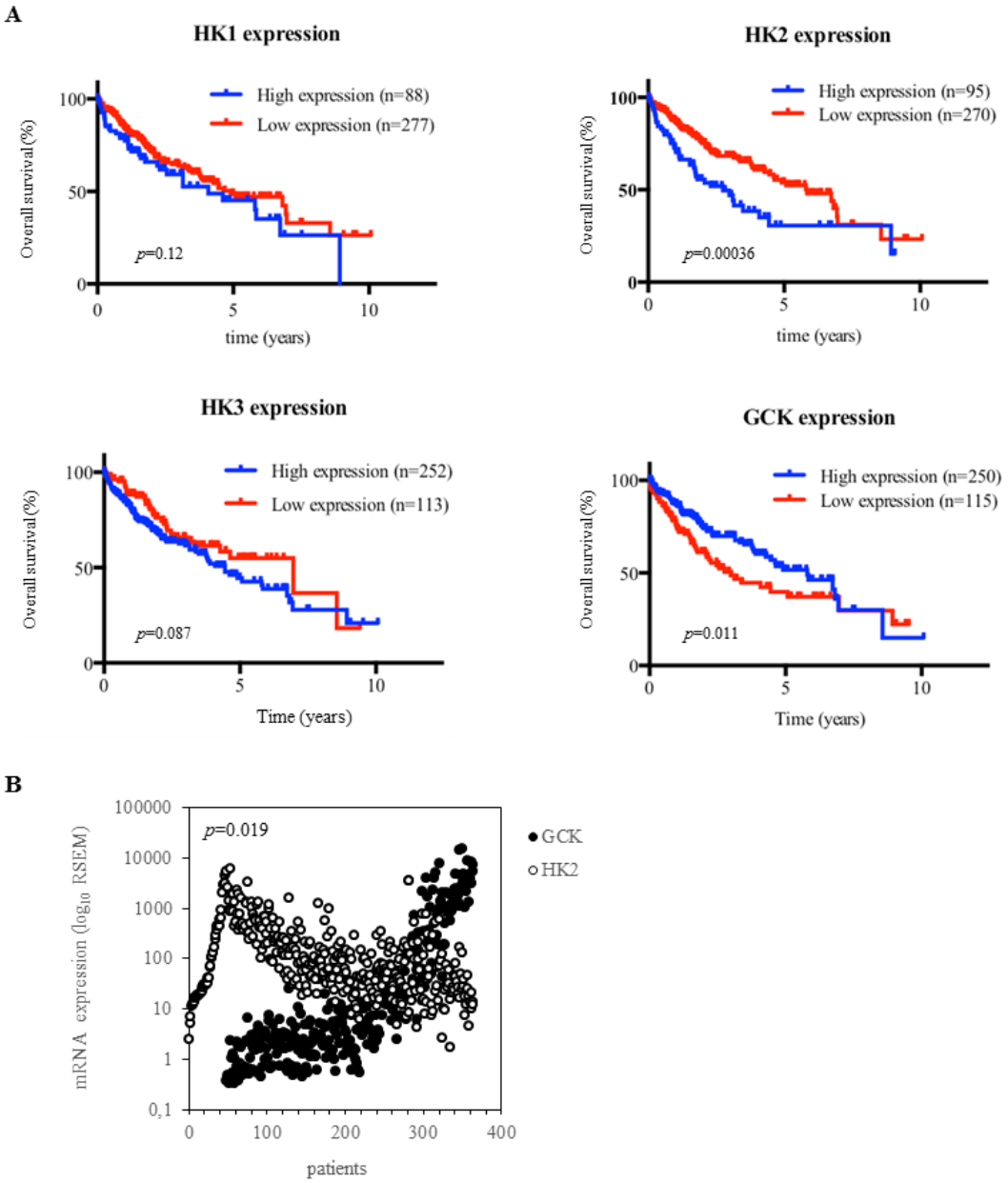

Figure 1. Correlation between hexokinase expression levels in HCC tumors and patients' survival. (A) Kaplan–Meier estimates of the survival of HCC patients depending on the expression of HK1, HK2, HK3 and GCK (HK4) genes in tumor biopsies (n=365). Optimal stratification between low and high expression groups was determined based on RNA-Seq gene expression data. Cut offs were set at 3.8, 1.4, 0.36, and 0.015 for HK1, HK2, HK3, and GCK, respectively. (B) GCK and HK2 expression levels across HCC biopsies from patients (Data from The Cancer Genome Atlas (TCGA) analyzed with cBioPortal (55, 56). Patients were ranked by increasing GCK/HK2 expression ratios. Spearman's correlation test, *p*-value=0.019.

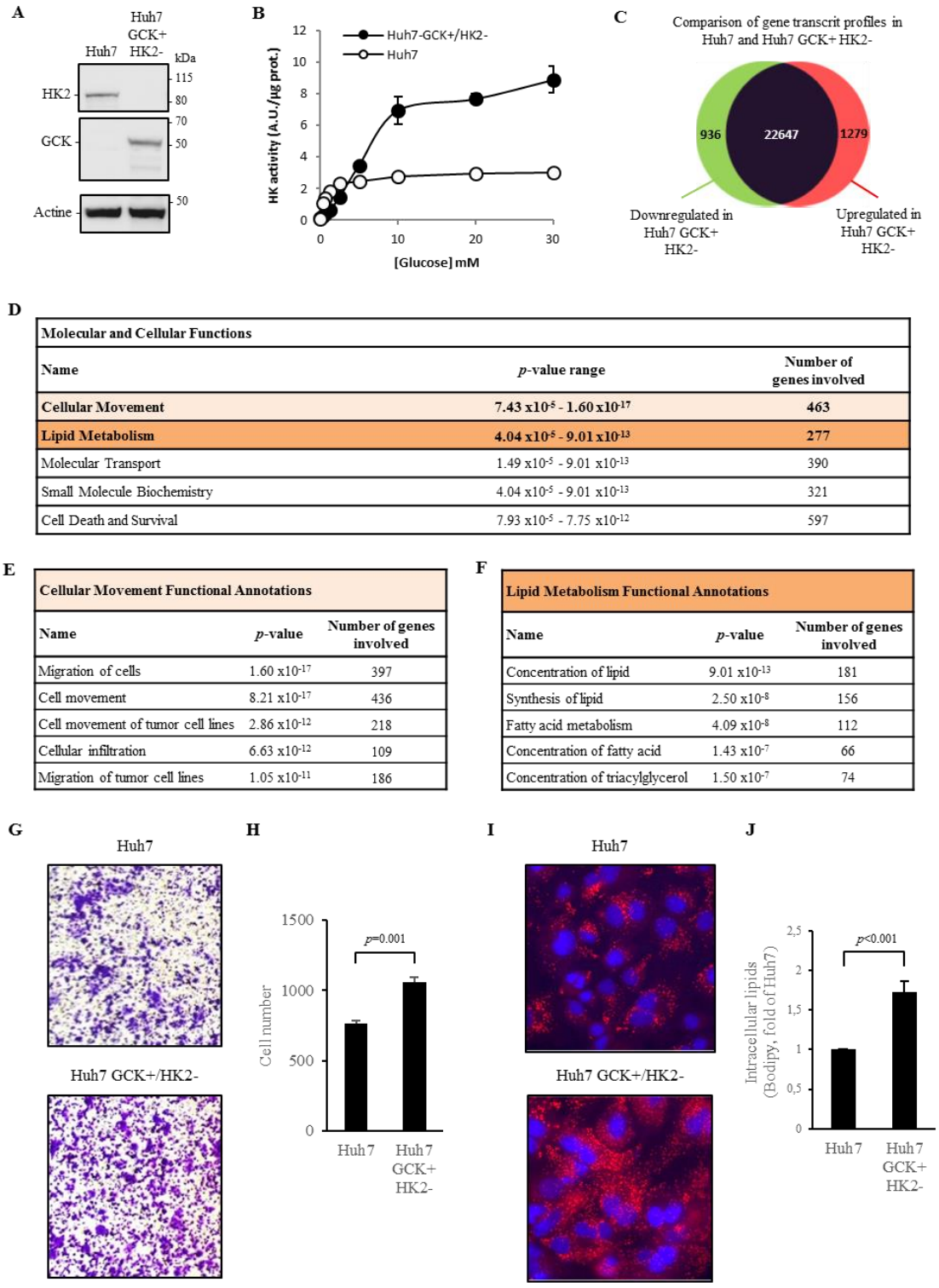

D

Molecular and Cellular Functions		
Name	***p*-value range**	**Number of genes involved**
Cellular Movement	**7.43×10^{-5} - 1.60×10^{-17}**	**463**
Lipid Metabolism	**4.04×10^{-5} - 9.01×10^{-13}**	**277**
Molecular Transport	1.49×10^{-5} - 9.01×10^{-13}	390
Small Molecule Biochemistry	4.04×10^{-5} - 9.01×10^{-13}	321
Cell Death and Survival	7.93×10^{-5} - 7.75×10^{-12}	597

E

Cellular Movement Functional Annotations		
Name	***p*-value**	**Number of genes involved**
Migration of cells	1.60×10^{-17}	397
Cell movement	8.21×10^{-17}	436
Cell movement of tumor cell lines	2.86×10^{-12}	218
Cellular infiltration	6.63×10^{-12}	109
Migration of tumor cell lines	1.05×10^{-11}	186

F

Lipid Metabolism Functional Annotations		
Name	***p*-value**	**Number of genes involved**
Concentration of lipid	9.01×10^{-13}	181
Synthesis of lipid	2.50×10^{-8}	156
Fatty acid metabolism	4.09×10^{-8}	112
Concentration of fatty acid	1.43×10^{-7}	66
Concentration of triacylglycerol	1.50×10^{-7}	74

Figure 2. Hexokinase isoenzyme switch in Huh7 cells modifies their migration capacity and lipid metabolism. (A) Western-blot analysis of HK2 and GCK expression in Huh7 and Huh7-*GCK*$^{+}$/*HK2*$^{-}$. (B) Hexokinase activity in homogenates of Huh7 and Huh7-*GCK*$^{+}$/*HK2*$^{-}$ cells. (C) Number of genes

changing their expression pattern in Huh7 and Huh7-*GCK*$^{+}$/*HK2*$^{-}$ cells (see Table S2 for details). Genes with FPKM<0.01 in both cell lines were not considered. (D) Analysis of differentially expressed genes in the two cell lines using gene set enrichment analysis (|FC|>2 with a *p*-value<0.05). Top five enriched molecular and cellular functions are presented. (E) and (F) Ranked IPA-annotations associated with 'cellular movement' and 'lipid metabolism'. (G-H) Results of transwell-migration tests. (G) Representative images and (H) count of migrating cells. (I) Oil Red-O staining of lipid droplets (red) with nucleus counterstaining (blue). (J) Quantification of intracellular lipids by FACS after BODIPY staining. H and J correspond to means ± SEM with n≥3 (*p*-value determined by Student's t-test).

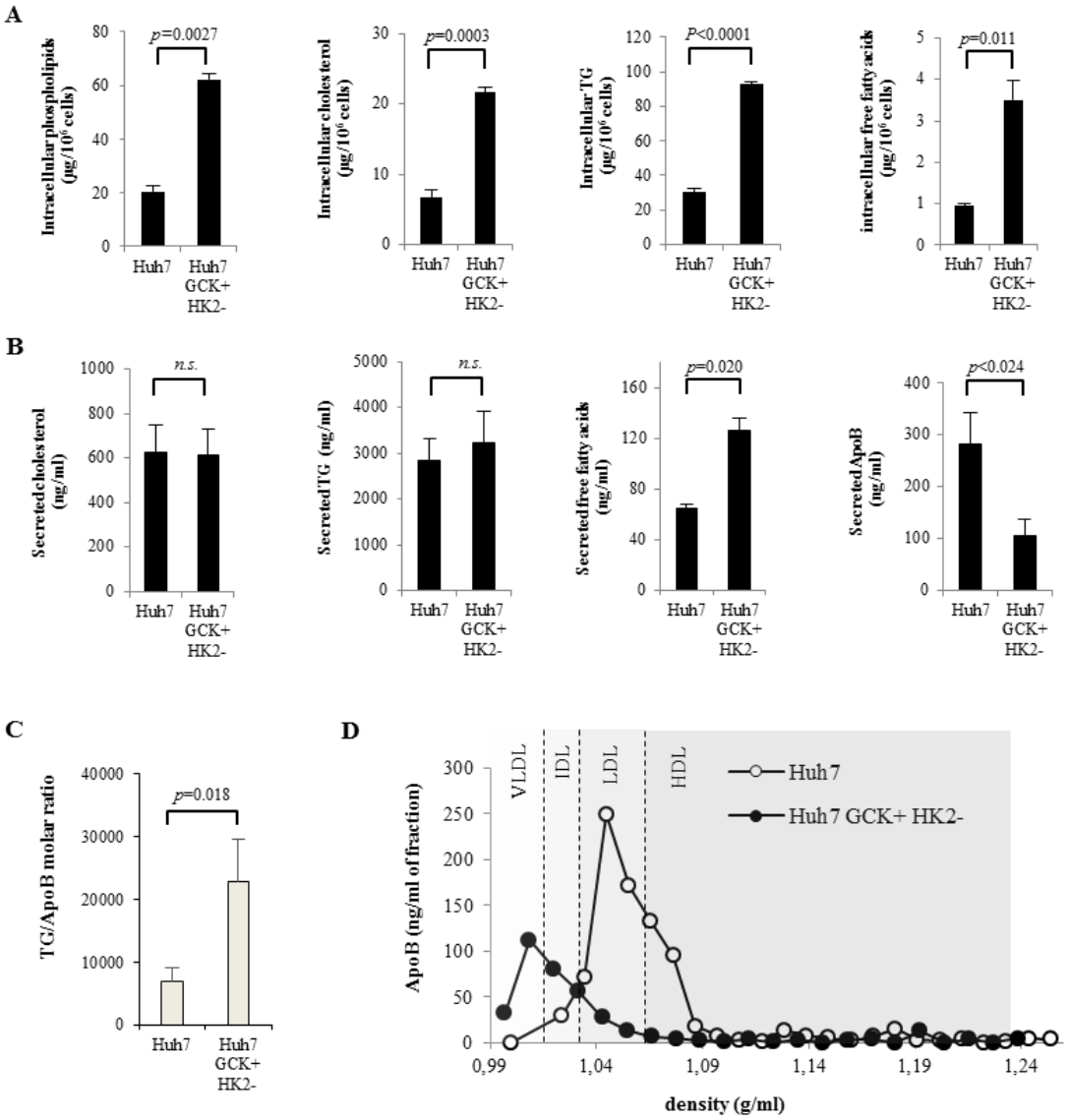

Figure 3. Lipogenesis and VLDL secretion is restored in Huh7-*GCK*$^{+}$/*HK2*$^{-}$ cells. (A) Quantification of intracellular lipids in total cell extracts of Huh7 and Huh7-*GCK*$^{+}$*HK2*$^{-}$ cells. (B) Lipids and ApoB secretions in supernatants of cells cultured 24h without FCS. (C) TG/ApoB molar ratio calculated from quantifications determined in (B). (D) Supernatants of Huh7 and Huh7-*GCK*$^{+}$/*HK2*$^{-}$ were analyzed by ultracentrifugation on iodixanol density gradients. ApoB was quantified in each fraction by ELISA. Presented data correspond to means ± SEM (n≥3, *p*-value determined by Student's t-test) except for (D) that shows one representative experiment.

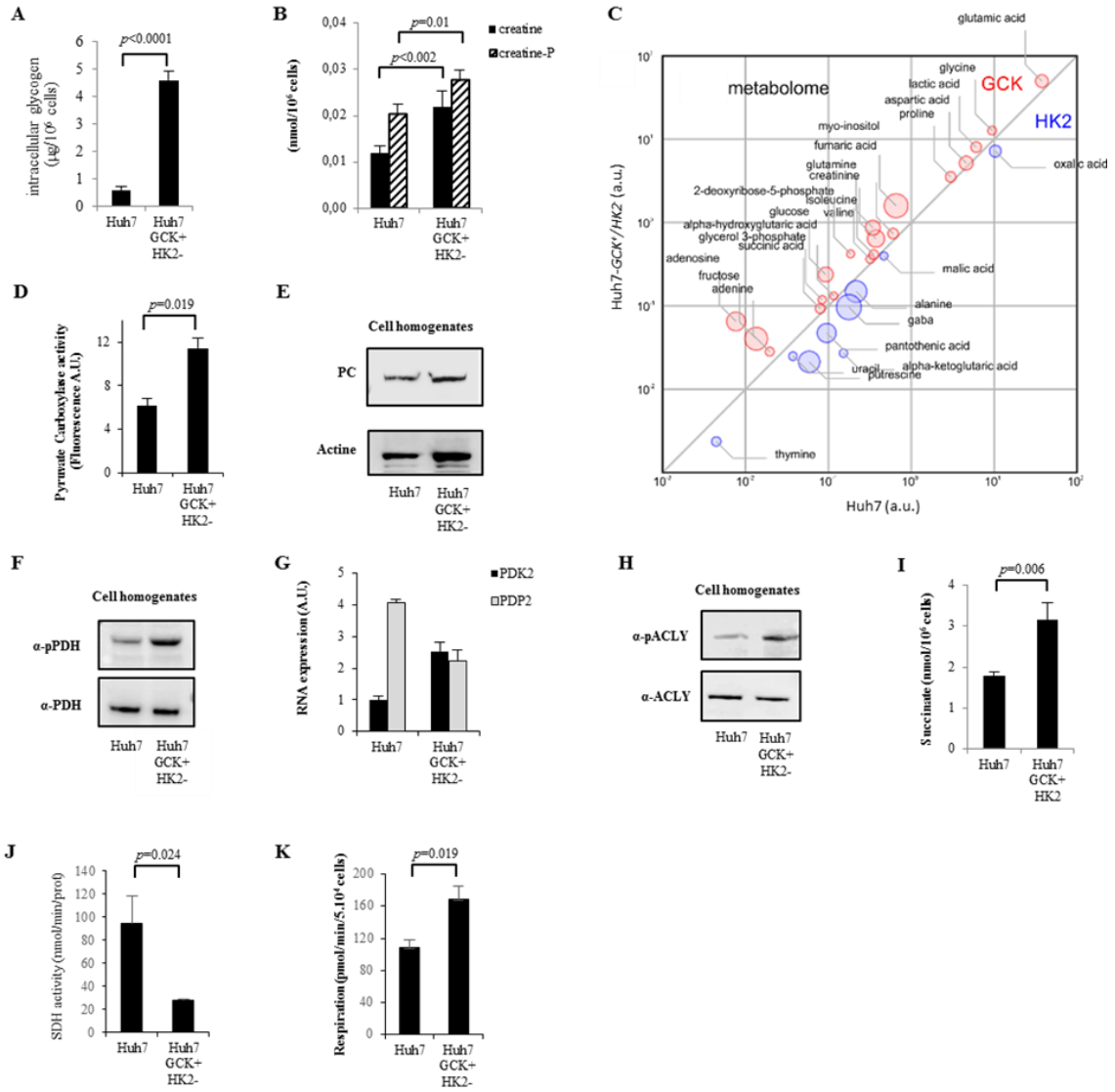

Figure 4. TCA rewiring after hexokinase isoenzyme switch in Huh7 cells. (A) Glycogen quantification. (B) Creatinine and creatinine-P quantification. (C) This bubble chart compares intracellular metabolomes of Huh7 and Huh7-*GCK*$^{+}$/*HK2*$^{-}$ cells. Metabolite pool sizes larger in Huh7 are indicated in blue, whereas the one larger in Huh7-*GCK*$^{+}$/*HK2*$^{-}$ are shown in red. The area of bubbles inversely scales with p-values between 5.10-2 and 1.10-17 of differential metabolomics responses. (D) Pyruvate carboxylase (PC) activity determined in cell homogenates. (E) Western-blot analysis of PC expression in Huh7 and Huh7-*GCK*$^{+}$/*HK2*$^{-}$ cells. (F) Western-blot analysis of pyruvate dehydrogenase (PDH) E1-alpha subunit phosphorylation at Ser293. (G) RNAseq quantification of pyruvate dehydrogenase kinase 2 (PDK2) and pyruvate dehydrogenase phosphatase 2 (PDP2)(BH p-value<0.05 from transcriptomic data). (H) Western-blot analysis of ATP-citrate Lyase (ACLY) phosphorylation at Ser455. (I) Succinate quantification in cell homogenates. (J) Succinate dehydrogenase (SDH) activity determined in cell homogenates. (K) Quantification of oxygen consumption rate. Data correspond to means ± SEM (n=3).

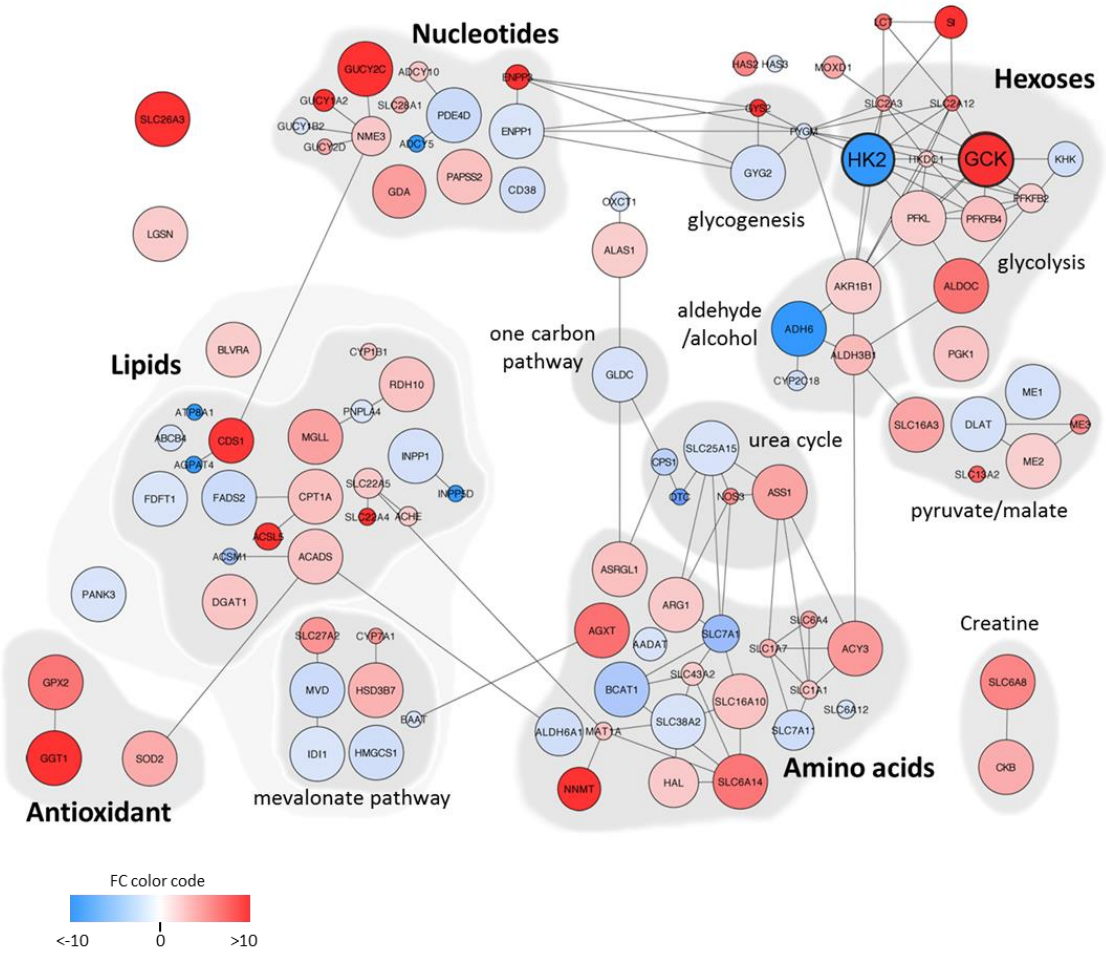

Figure 5. Gene-centric analysis of metabolic pathways affected by the hexokinase isoenzyme switch. Clusters of metabolism-associated genes that are either up (red) or downregulated (blue) in Huh7-*GCK*$^{+}$/*HK2*$^{-}$ vs Huh7 cells were extracted from transcriptomic data using HepatoNet1 as framework (|FC|>2; p-value<0.05). Edges connect cellular genes coding enzymes that have at least one metabolite in common, either as substrate or product. Grey areas delimitate clusters of genes belonging to the same metabolic module.

A

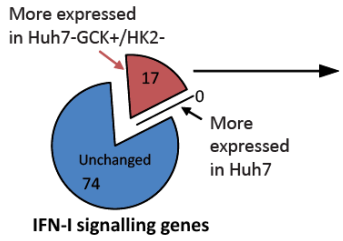

B

Gene ID	Huh7 (median FPKM)	Huh7-GCK+/HK2- (median FPKM)	FC
IRF1	1,38	4,03	2,93
IRF9	2,07	6,23	3,01
IRF7	0,01	0,38	26,05
MX1	0,38	1,01	2,65
OAS1	0,29	6,41	21,84
OAS3	0,86	5,46	6,35
IKBKE	1,28	14,46	11,29
IFI6	1,32	10,70	8,14
IFITM3	7,38	45,98	6,23
IFI35	1,34	7,49	5,58
EGR1	2,21	6,52	2,94
PSMB8	0,23	5,70	24,47
GBP2	1,84	6,14	3,33
MDA5	0,28	0,93	3,28
HLA-H	2,43	7,78	3,20
HLA-A	6,16	16,36	2,65
RNASEL	0,01	0,04	4,20

C

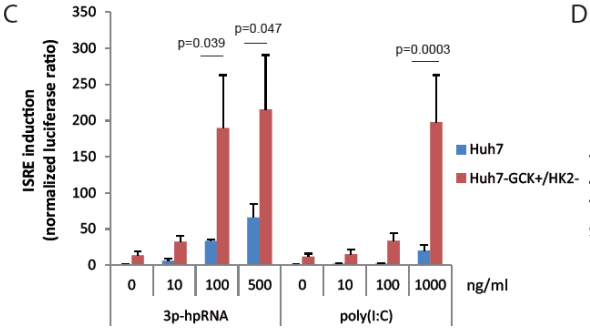

D

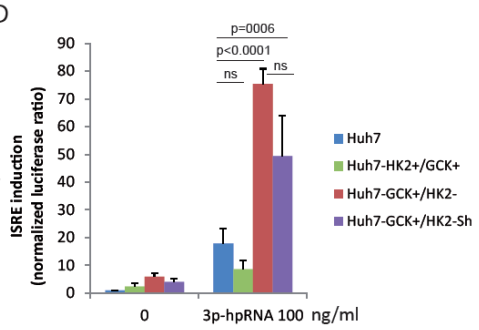

E

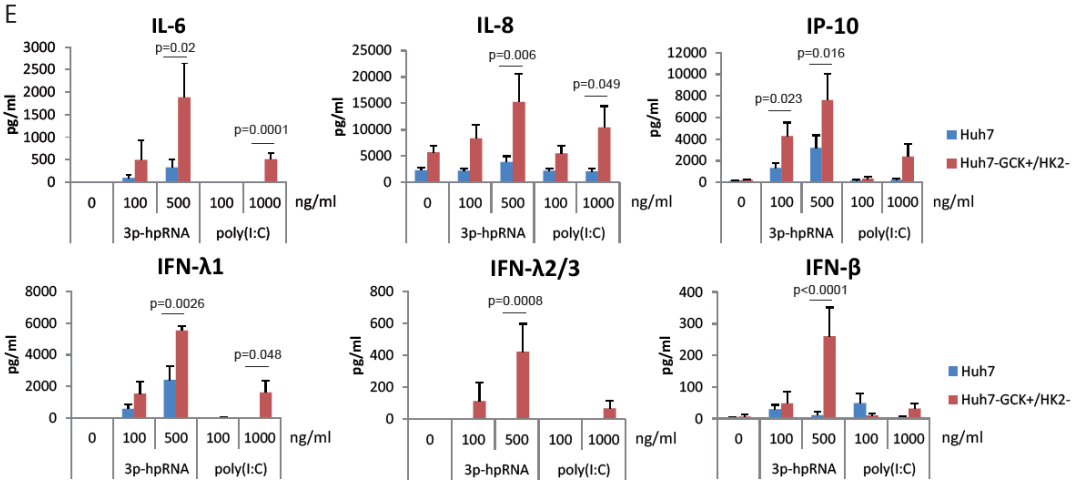

F

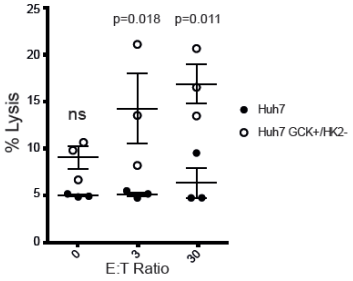

Figure 6. Innate immune response is enhanced in Huh7-GCK+/HK2- cells. (A-B) Sector chart from the transcriptomic study showing genes included in the GO-term "Type I-IFN signaling pathway". (C) List of 17 genes significantly up-regulated (|FC|>2, BH p-value<0.05) in Huh7-*GCK*$^{+}$*/HK2*$^{-}$ compared to Huh7 cells. (C-E) Cells were stimulated or not for 48h with 3p-hpRNA (RIG-I ligand) or poly(I:C) (MDA5 ligand). ISRE-luciferase expression was monitored and normalized to Renilla luciferase (C-D). Cell supernatants were assayed for cytokine concentration by multiplex assays (E). (F) NK cell mediated lysis of Huh7 or Huh7-*GCK*$^{+}$*/HK2*$^{-}$. Hepatoma cells were seeded 24h before NK cells addition for 4h at effector to target (E:T) ratio of 0, 3 or 30. After harvesting, cell lysis was determined by the percentage of PI+ cells on gated hepatocytes. p-values were obtained from 2-way ANOVA analyses comparing matched cell means with Sidak's correction for multiple comparison, with α=0.05.

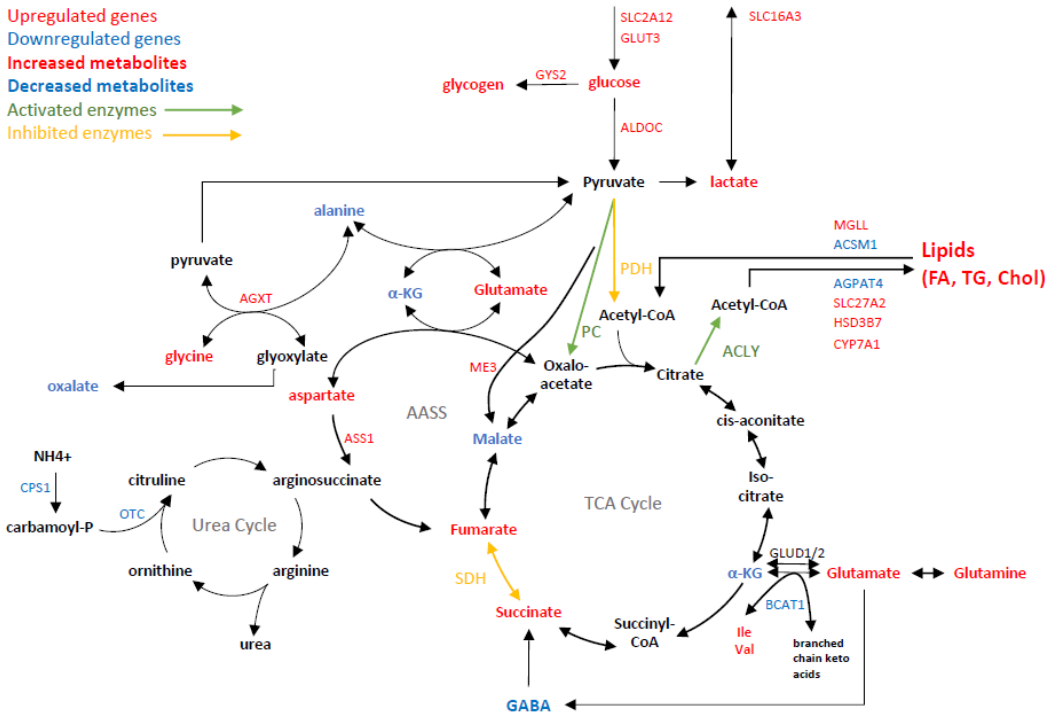

Figure 7. Simplified scheme of central carbon metabolism and connected pathways showing differences between Huh7-*GCK*$^{+}$/*HK2*$^{-}$ vs Huh7. Highlighted metabolites, enzymatic activities, and metabolism-associated genes were selected from metabolomic (Fig. 4C), enzymatic (Fig. 4D-J), and transcriptomic analyses (Fig. 5).